ANALYSIS OF OPTIMAL ROLL TENSIONING FOR CIRCULAR SAW STABILITY

G. S. Schajer
Research Engineer
Weyerhaeuser Company, Tacoma, WA 98477

and

C. D. Mote, Jr.
Professor
Department of Mechanical Engineering, University of California
Berkeley, CA 94720

(Received September 1982)

ABSTRACT

When a circular saw is used to cut wood, a substantial and increasingly important fraction of the raw material is wasted because of the excessive width of the sawcut. The process of "roll tensioning" is studied here, whereby sawblade thickness, and hence material loss, can be significantly reduced while still maintaining sawblade stability. A theoretical model is developed that accurately describes the localized plastic deformation that takes place during roll tensioning, the associated residual stresses, and the resulting changes in sawblade natural frequencies. Experimental measurements of the residual stresses and natural frequencies confirm the theoretical predictions. The mathematical model allows reliable prediction of optimal tensioning conditions for any given saw operating state and development of automated control of the tensioning process. An example is presented in which the thickness of an optimally tensioned circular sawblade is 33% smaller than the thickness of an untensioned sawblade of equivalent transverse stability.

Keywords: Tensioning, circular saw, rolling contact, roller deformation, rotating disc, natural frequency, critical speed.

LIST OF SYMBOLS

A = cross-sectional area of indentation on each side of disc
a = radius of disc central hole
b = peripheral radius of disc
E = Young's modulus
F = roller force
h = disc half-thickness
k_1, k_3 = dimensionless compliance factors
N = number of roller circuits around disc
n = nodal diameter vibration mode number
r = general radius
r_i = inner radius of region II
r_m = mean radius of region II = $(r_i + r_o)/2$
r_o = outer radius of region II
S_1, S_3 = radial stresses at boundaries of region II
α, β = constants in equation (12)
γ, λ = constants in equations (13) and (14)
ϵ = radial strain

Wood and Fiber Science, 16(3), 1984, pp. 323–338

ϵ_z = transverse strain
ϵ_θ = circumferential strain
ϵ^*_θ = limiting circumferential plastic strain
σ_r = radial stress
σ_z = transverse stress
σ_θ = circumferential stress
σ_o = yield stress of disc material
ν = Poisson's ratio
Ω = disc rotation speed, rad/sec
ω_n = disc natural frequency, rad/sec

Superscript ′ denotes elastic component of deformation
Superscript ″ denotes plastic component of deformation

INTRODUCTION

The circular saw is one of the most widely used industrial cutting tools, and has many diverse applications ranging from meat cutting in the butchery trade to slicing of silicon wafers in the microelectronics industry. In almost all cases, the amount of material lost during each sawcut is of major and increasing importance. In the forest products industry, about 12% of the wood cut in sawmills is reduced to sawdust. A further 7% of the material is subsequently lost as planer shavings (Harpole et al. 1979). This represents a substantial economic loss in a process where the raw material now accounts for 72% of total costs (Clephane and Carroll 1981).

Sawcut losses can be significantly reduced by decreasing sawblade thickness. However, a large saw thickness reduction cannot usually be made without impairing the transverse stability of the blade and the accuracy of the cut. This adverse behavior is a resonance phenomenon associated with the onset of critical speed instability (Mote and Nieh 1973). For over one hundred years, skilled craftsmen have "tensioned" their circular saws to improve blade stability, traditionally by hammering the surfaces in specific patterns determined by experience (Dugdale 1966). In the more modern roll tensioning process, the sawblade is locally deformed between two opposing pinch rollers, as shown in Fig. 1. The rollers compress the sawblade such that yielding of the blade material occurs in the contact zone. One or both rollers are then driven, causing the sawblade to rotate slowly and a shallow groove to be formed on each side of the blade at a constant radius. The localized deformation caused by this rolling induces residual stresses within the sawblade, and it is the presence of these in-plane stresses that modifies the blade natural frequencies and critical speed.

Since instability occurs when the saw rotation speed is close to the critical speed, it is the purpose of tensioning to increase the critical speed away from the rotation speed (Mote and Nieh 1973). In contrast, thickness reduction of a sawblade lowers the critical speed and decreases saw stability. The roll tensioning technique is much more consistent and repeatable than the hammer method, and has very important potential for automation and computer control. At present, however, control of the process is based on the judgment and experience of the craftsman, and the results can be very variable.

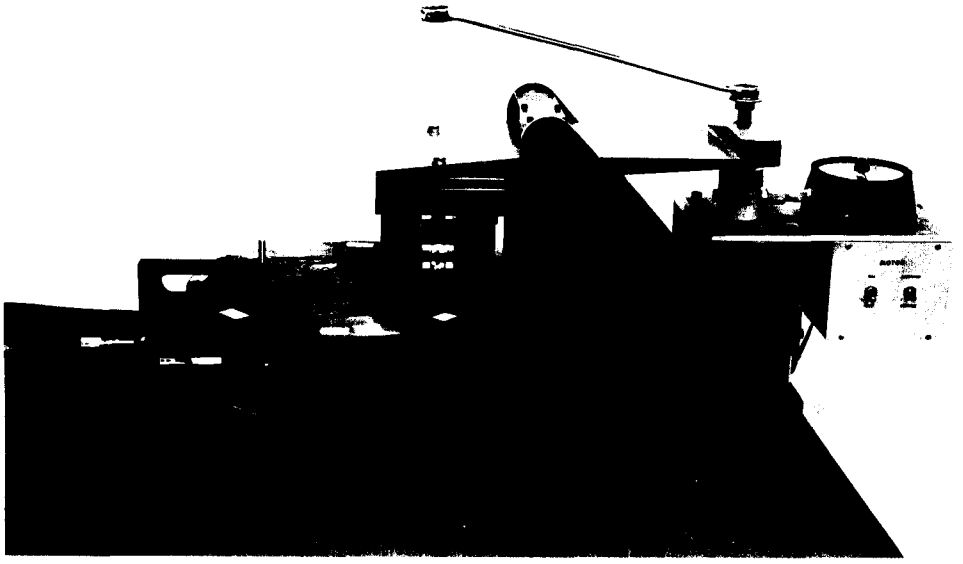

FIG. 1. Instrumented roll tensioning machine.

The objective of this study is to establish the relationship between the process of circular saw tensioning and the resulting change in sawblade stability. This relationship is shown diagramatically in Fig. 2. Once the steps in Fig. 2 have been analytically described, it is then possible to consider the question of optimal tensioning. This is done here, and an example is given in which optimal tension conditions are predicted. It is shown that, through optimal tensioning, a 33% reduction in thickness can be achieved compared with an untensioned sawblade of equivalent transverse stability.

THEORY

A roll-tensioned sawblade is modelled as a circular disc, divided into the three annular regions shown in Fig. 3. Region II represents the plastically deformed material in the roller path, and regions I and III represent the adjacent elastically deformed material. The saw teeth do not appear in the model because they have little influence on the natural frequencies of a circular saw.

The evaluation of the radial stresses S_1 and S_3 at the boundaries of region II is the key to the residual stress analysis. Once these stresses have been determined, the stress distribution in all three regions of the model can be directly calculated. No constraint is imposed on the magnitudes of S_1 and S_3, and in general, either of them may be tensile or compressive. Similarly, no constraint is imposed on the magnitudes or signs of the plastic strains in the roller path. The material that is compressed between the rollers may deform both radially and circumferentially.

Because the plastic deformations are small, both the elastic and plastic strains

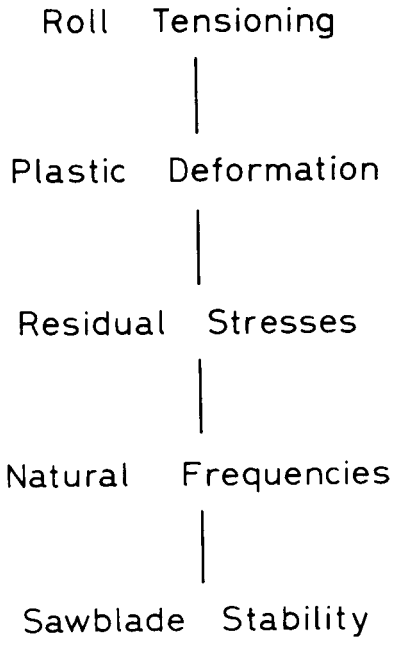

FIG. 2. Conceptual relationship between the roll tensioning of a circular sawblade and its operational stability.

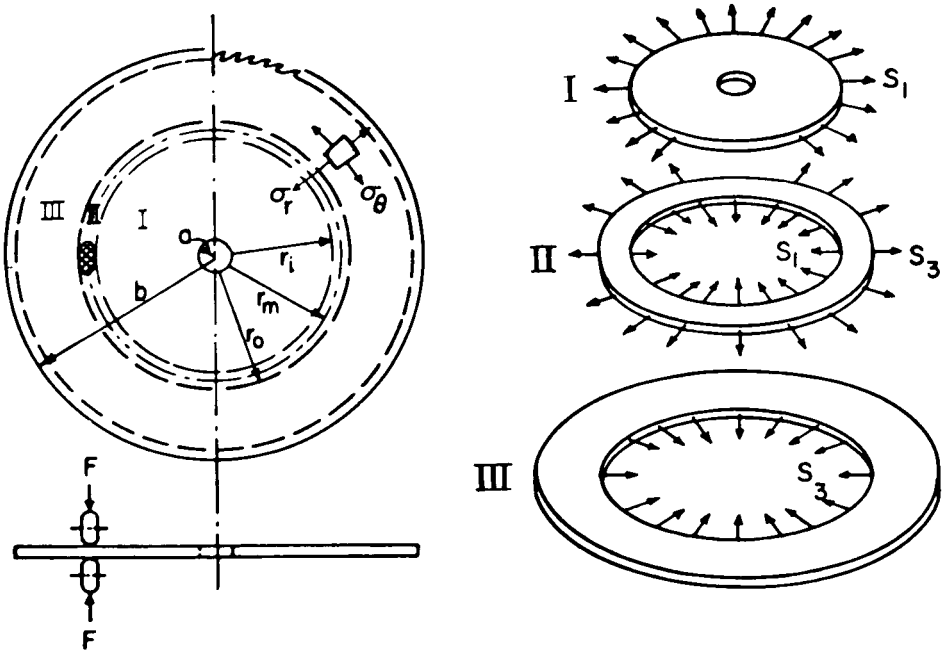

FIG. 3. Three-region theoretical model of a rolled circular sawblade. After Szymani and Mote (1979).

must be considered. Elastic strain components are denoted ϵ', plastic components ϵ'', and total strains $\epsilon = \epsilon' + \epsilon''$. The plastic strain components obey the constant-volume plasticity condition

$$\epsilon''_\theta + \epsilon''_r + \epsilon''_z = 0 \tag{1}$$

where the subscripts refer to the circumferential, radial, and transverse directions, respectively. All stresses are assumed uniform through the sawblade thickness.

The solutions for the stresses in regions I and III in terms of S_1 and S_3 follow directly from the classical Lamé equations for an axi-symmetric system. The circumferential and radial stresses at radius r in region I are

$$\sigma_\theta = S_1 \frac{r_i^2}{r_i^2 - a^2}\left(1 + \frac{a^2}{r^2}\right), \qquad \sigma_r = S_1 \frac{r_i^2}{r_i^2 - a^2}\left(1 - \frac{a^2}{r^2}\right) \tag{2}$$

and in region III are

$$\sigma_\theta = S_3 \frac{r_o^2}{r_o^2 - b^2}\left(1 + \frac{b^2}{r^2}\right), \qquad \sigma_r = S_3 \frac{r_o^2}{r_o^2 - b^2}\left(1 - \frac{b^2}{r^2}\right) \tag{3}$$

where the radii a, r_i, r_m, r_o and b are shown in Fig. 3 (Schajer 1981). Given that the width of region II is very small compared with its mean radius, the radial stresses there are small compared with the circumferential stresses, and may be neglected. The stresses in region II are then

$$\sigma_\theta \simeq \frac{(S_3 - S_1)r_m}{r_o - r_i}, \qquad \sigma_r \simeq 0 \tag{4}$$

Compatibility of radial displacements at the boundaries of region II with regions I and III gives the relationship between the stresses S_1 and S_3 and the plastic deformation within the roller path (Schajer 1981).

$$S^1 = \frac{(1 - \nu - k_3)\int_{r_i}^{r_o} \epsilon''_\theta \, dr + \int_{r_i}^{r_o} \epsilon''_z \, dr}{r_m(k_1 - k_3)/E} \tag{5}$$

$$S_3 = \frac{(1 - \nu - k_1)\int_{r_i}^{r_o} \epsilon''_\theta \, dr + \int_{r_i}^{r_o} \epsilon''_z \, dr}{r_m(k_1 - k_3)/E} \tag{6}$$

where k_1 and k_3 are dimensionless factors representing the radial compliance (radial displacement/radial stress) of regions I and III at the boundaries with region II.

$$k_1 = \frac{(1 - \nu)r_i^2 + (1 + \nu)a^2}{r_i^2 - a^2} \tag{7}$$

$$k_3 = \frac{(1 - \nu)r_o^2 + (1 + \nu)b^2}{r_o^2 - b^2} \tag{8}$$

The plastic strain components in Eqs. (5) and (6) can be determined by integrating the flow rule associated with the yield characteristic of the sawblade material. For the conditions considered here, and using the von Mises yield criterion, (Hill 1950), a simple approximate solution for ϵ''_θ in terms of ϵ''_z is

$$\frac{\epsilon''_\theta}{\epsilon^*_\theta} = 1 - e^{\epsilon''_z/2\epsilon^*_\theta} \tag{9}$$

where

$$\epsilon^*_\theta = \frac{\sigma_o}{\sqrt{3}E} \simeq 0.58\sigma_o/E \tag{10}$$

This approximation gives ϵ''_θ values within 4% of those from the exact solution (Schajer 1981).

The flow rule associated with the Tresca yield criterion predicts that the plastic deformation of the material in the roller path is purely radial. This differs from the prediction of the von Mises criterion where a finite circumferential plastic strain ϵ''_θ is also predicted. For typical rolling conditions such as $\epsilon''_z/\epsilon^*_\theta < -6$, then $\epsilon''_\theta < 0.2\epsilon''_r$. This roll tensioning model is a rare case where the choice of yield criterion makes a significant difference to the predicted stresses, even though the predicted plastic strains do not differ substantially. The experimental measurements made during this study show that the yield behavior during rolling of the specimen sawblade steel[1] is more closely modelled by the von Mises yield criterion than by the Tresca criterion. This intermediate behavior between the two yield criteria, with a bias towards the von Mises, is consistent with the results of Taylor and Quinney (1931) who measured the yield characteristics of various metals under multiaxial loading conditions.

In this study, the unknown effects of friction in the roller contact zone and nonuniformities in the plastic deformation through the sawblade thickness make it difficult to draw firm conclusions about the precise nature of the yield criterion of the sawblade material used. For the purpose of this analysis only, a modified material plastic deformation characteristic is proposed. Equation (9) can be applied to the predictions of both the von Mises and Tresca Yield criteria by setting $\epsilon^*_\theta = 0.58\sigma_o/E$ or $\epsilon^*_\theta = 0$, respectively. The empirically determined intermediate value

$$\epsilon^*_\theta = 0.4\sigma_o/E \tag{11}$$

gives good correspondence between the predicted plastic strains in the roller path and those in experiments with rolled sawblade plates.

ROLL TENSIONING

An experimental program was undertaken to investigate the steps in the tensioning process sequence outlined in Fig. 2. The instrumented roller machine shown in Fig. 1 was used for the experimental measurements. The roller load was

[1] Specification 55—Alloy Steel, Crucible Steel Company of America, hardened to 42 Rc. Yield stress, $\sigma_o = 1{,}280$ N/mm^2.

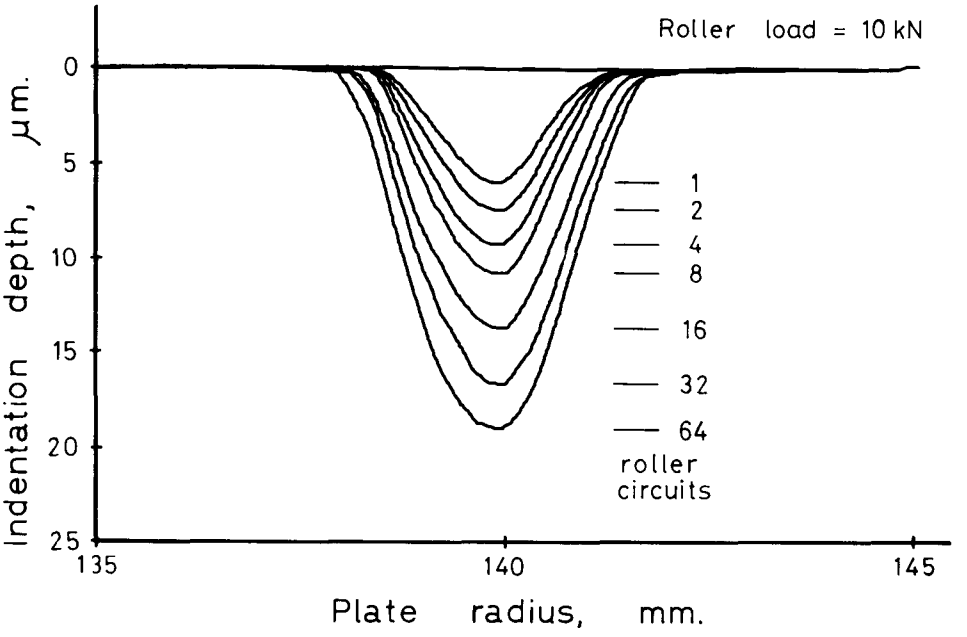

FIG. 4. Indentation profiles after repeated rolling at 10 kN load.

applied through a lever and screw mechanism, and the magnitude of the load was measured using a hydraulic load cell. The rollers were designed to have "spherical" geometry, that is, the crowning radius and the roll radius were both 42.5 mm. Initially stress-free circular discs, 200-mm radius with a 16-mm radius hole, made of Specification 55 sawblade steel, were used as specimens.

Two precision differential transformer displacement transducers were fixed in the yoke shown on the left of Fig. 1, one above and one below the disc. The yoke was in turn mounted on a small traverse driven by a stepper motor. A PDP 8/E laboratory computer controlled the position of the stepper motor and also took measurements from the displacement transducers. The transducers were electrically balanced and serially connected so that they were sensitive to relative displacements only. Roller indentation profiles across the roller path were obtained from thickness measurements taken at regular increments across the path, typically 101 measurements at 0.1-mm intervals. Also, the discs were initially polished along the paths of the thickness measurements to reduce the 3 μm irregularity in readings due to surface grinding marks to less than 0.5 μm. Resolution and repeatability of the measurements showed errors less than 0.2 μm.

In the first series of experiments, the roller path thickness profile was measured as a function of roller load, roller path position and number of roller traversals over the same path. Measurements were made using 5 kN, 10 kN and 15 kN roller loads and with mean roller path radii, r_m = 110 mm, 140 mm and 170 mm. In all cases the discs were 2 mm thick. Roller path thickness profiles were measured after 1, 2, 4, 8, 16, 32 and 64 roller circuits or until disc buckling prevented further rolling.

Figure 4 shows a typical series of indentation profiles for increasing numbers

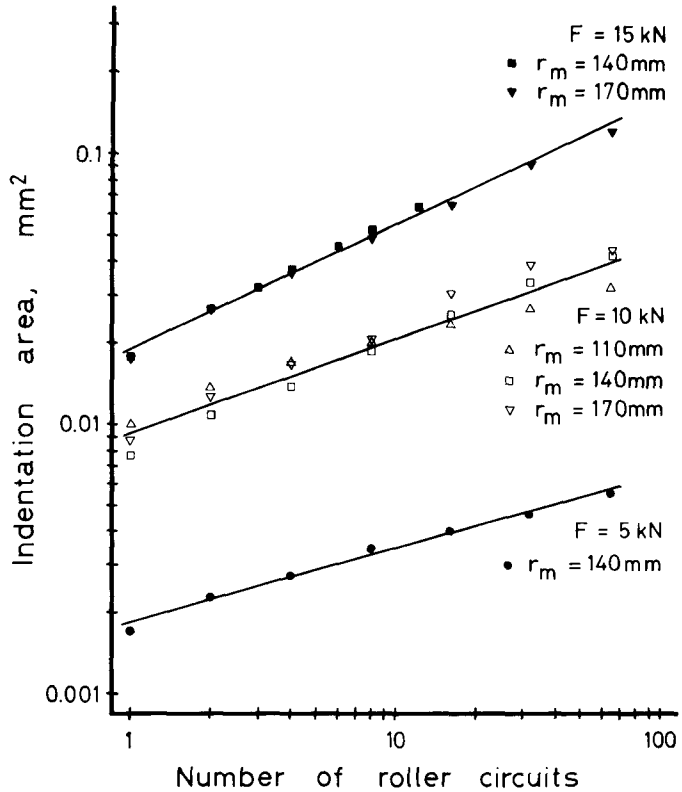

FIG. 5. Measured roller path indentation areas for rolling at different roller path radii.

of roller circuits with a constant 10 kN roller load. Substantial deformation takes place during the initial circuit, and continues during subsequent circuits, although at a steadily diminishing rate. This increase in indentation after repeated rolling is due to the changing shape of the roller-disc contact area. During the first circuit, each roller moves over a flat surface, while on subsequent circuits over the same path, the rollers move along increasingly curved grooves. In contrast to rolling a material that is thick compared with the contact diameter, there is no "piling up" of deformed material on the sides of the roller path. This is because the lateral material constraint on the contact zone is much reduced in a thin plate.

Figure 5 shows the measured roller path indentation areas for the three roller loads and the three roller path radii as a function of number of roller circuits around the disc. The indentation area is the mean of the cross-sectional areas of the indentation on each side of the plate and equals the area enclosed by the corresponding curve in Fig. 4. This deformation measure was chosen because it includes the effects of both the depth and width of the roller path indentation. The data show that the indentation area vs. the number of roller circuits relationships are almost independent of the radial position of the roller path, although there is some scattering of the data points. This scattering is due to the extreme sensitivity of the results to the alignment precision of the rollers, particularly for the lower roller loads. For example, it was found that the rotation axes of the

rollers had to be adjusted parallel to each other to within 0.2° (angle measured in the plane parallel to the disc surface); otherwise unsymmetrical indentation profiles were formed.

For the range investigated, the measured indentation area is closely approximated by a power-law relationship

$$A = \alpha N^{\beta} \tag{12}$$

where N is the number of roller circuits and

$$\alpha = 0.0017 \text{ mm}^2, \quad \beta = 0.27 \text{ for } 5 \text{ kN roller load},$$
$$\alpha = 0.008 \text{ mm}^2, \quad \beta = 0.42 \text{ for } 10 \text{ kN roller load},$$
$$\alpha = 0.019 \text{ mm}^2, \quad \beta = 0.50 \text{ for } 15 \text{ kN roller load}.$$

In an approximate theoretical analysis, where the disc material was idealized as rigid-perfectly plastic and the rollers perfectly rigid (Schajer 1981), a similar power-law relationship was predicted with the exponent $\beta = 0.75$. The measured exponents are lower than this idealized value because of the elastic deformations of the disc and the rollers. As the roller load is decreased, the plastic strains in the contact zone diminish relative to the elastic strains and the elastic deformations become more significant in the modelling.

The constant α in (12) corresponds to the indentation area after the first roller circuit. In the idealized rigid-plastic analysis, α is proportional to the roller load to the power 1.5. The exponent of the experimentally measured relationship is 2.2. This increase is also due to the elastic deformation of the sawblade plate and the rollers.

A second series of experiments was undertaken in order to examine the influence of disc thickness on roller path indentations during disc rolling. Three discs, 1.5, 2.0, and 2.5 mm thick, respectively, were rolled up to 64 times using a 15 kN roller load at $r_m = 170$ mm. All the measured indentation area vs. number of roller circuits data points very closely followed the 15 kN line in Fig. 5, showing that the deformation in the roller path is independent on the disc thickness. This behavior is expected from theory, providing that the disc thickness is small compared with the contact diameter.

PLASTIC DEFORMATION

The radial stresses S_1 and S_3, are calculated explicitly using Eqs. (5) and (6) when the strain components ϵ''_θ, ϵ''_r and ϵ''_z are known. As shown previously, the von Mises and Tresca yield criteria lead to different predictions for the relative magnitudes of these strain components and hence to different resulting stress distributions. It is helpful now to consider an extreme case, given that the roller path deformation is independent of roller path radius. Consider the rolling of a band saw, noting that it may be considered as an extreme case of a circular saw whose hole radius and peripheral radius are both very large and almost equal. For the band saw, the effects of the longitudinal and lateral plastic strains (equivalent to circumferential and radial strains in a circular saw) are decoupled and may be examined individually. The longitudinal strains in a band saw cause a lengthening of the plate and also the development of longitudinal residual (tensioning) stresses. The lateral strains, however, only cause a slight widening of the plate with no residual stress development.

A series of experiments was undertaken where rectangular plates of sawblade steel, 300 × 50 × 2.0 mm, were rolled longitudinally using the roller machine shown in Fig. 1. This machine was modified temporarily to accept these specimens. Three plates were rolled using 10 kN, 15 kN and 20 kN roller loads. The longitudinal extension and indentation profiles were measured for up to 64 roller traversals. Figure 6 shows the longitudinal extension as a function of indentation area. The predictions from the von Mises and Tresca yield criteria are also shown. These two lines were calculated by determining ϵ''_θ point by point from the measured indentation profile using Eq. (9) and either $\epsilon^*_\theta = 0.58\sigma_o/E$ or $\epsilon^*_\theta = 0$, and integrating across the width of the roller path. This calculation is described in detail by Schajer (1981). The measurements in Fig. 6 show that the material behavior in the roller path is not accurately described by either the von Mises or Tresca yield criteria, but lies between the predictions of the two models. Empirically, the intermediate "modified" value $\epsilon^*_\theta = 0.4\sigma_o/E$ gives good correspondence between the measured and predicted longitudinal extensions.

The results in Fig. 6 show that most of the tensioning effect during band saw rolling takes place during the early stages of the deformation, with comparatively little subsequent increase in longitudinal extension and tensioning stresses. Thus, it is more effective to roll a band saw with a low roller load over several adjacent roller paths, than to roll heavily over a single path.

RESIDUAL STRESSES

An empirical power-law relationship was fitted to the data represented by the "modified" curve in Fig. 6. This was incorporated into Eqs. (5) and (6) so that the radial stresses S_1 and S_3 can be directly calculated in terms of the roller path indentation area. The result is

$$S_1 = \frac{\left[\frac{1 - 2\nu - k_3}{2 - \nu}\left(\frac{\gamma - A/h}{\gamma}\right)^{\lambda} - 1\right]EA}{r_m(k_1 - k_3)h} \tag{13}$$

$$S_3 = \frac{\left[\frac{1 - 2\nu - k_1}{2 - \nu}\left(\frac{\gamma - A/h}{\gamma}\right)^{\lambda} - 1\right]EA}{r_m(k_1 - k_3)h} \tag{14}$$

where $\gamma = -0.0013$ mm and $\lambda = -0.8$ for the roller geometry and sawblade material used in these experiments. These two constants were determined through a least-squares minimization of error between the measured and predicted values in Fig. 6. The other symbols are defined in the symbol list. A detailed derivation of Eqs. (13) and (14) is given by Schajer (1981).

The predictions from Eqs. (13) and (14) were tested in an experiment in which strain gauges were used to monitor the growth of residual stresses in a rolled disc. The strain gauges were mounted on both sides of the roller path and also on both sides of the disc, so that the stresses S_1 and S_3 could be determined independent of any plate bending effects. The disc was successively rolled 32 times using

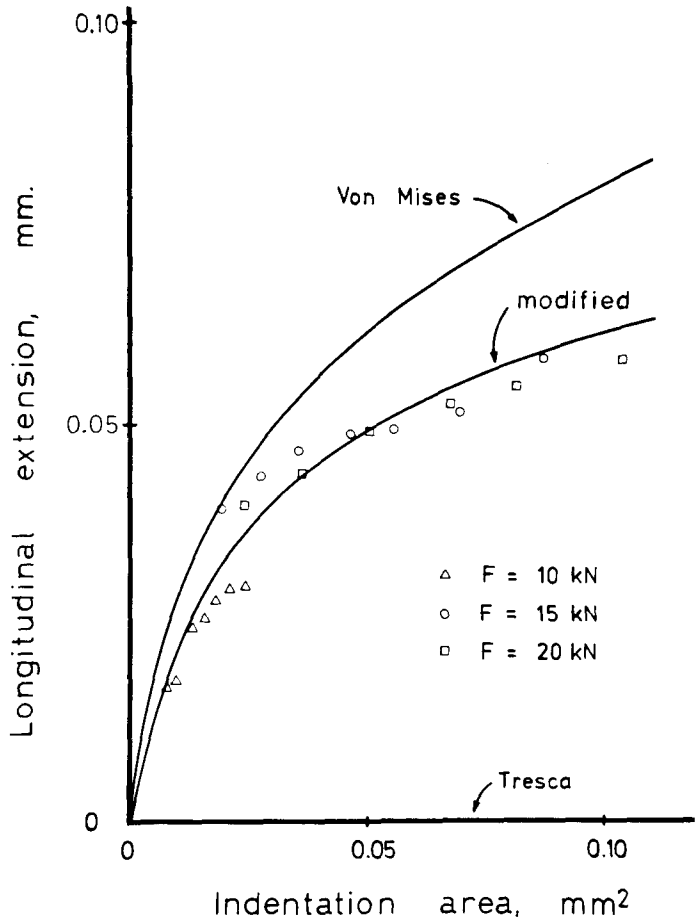

FIG. 6. Longitudinal extension vs. indentation area for a rolled rectangular plate.

4 kN, 5 kN and 7.5 kN roller laods. The laboratory computer took readings from the gauges for each load after 1, 2, 4, 8, 16 and 32 roller circuits around the disc and also measured the corresponding indentation profiles.

Figure 7 shows the relationship between the stresses S_1 and S_3 and the roller path indentation area. The agreement between the predicted and the experimental values is very good; the difference between the solid lines, which are calculated using Eqs. (5) and (6), and the experimental points is less than 2 N/mm^2. Also, the main features of the experimental results are correctly predicted. First, S_1 and S_3 are of different magnitudes, and second, S_1 is tensile for small indentation areas before becoming compressive after further deformation. These features of the stress distribution in a tensioned circular saw, which are due to the presence of large compressive stresses within the roller path, significantly influence the changes in sawblade natural frequencies due to rolling. They have been observed by other investigators (Kimura and Ando 1974; Pahlitzsch and Friebe 1973; Szymani and Mote 1979), but have not been previously explained.

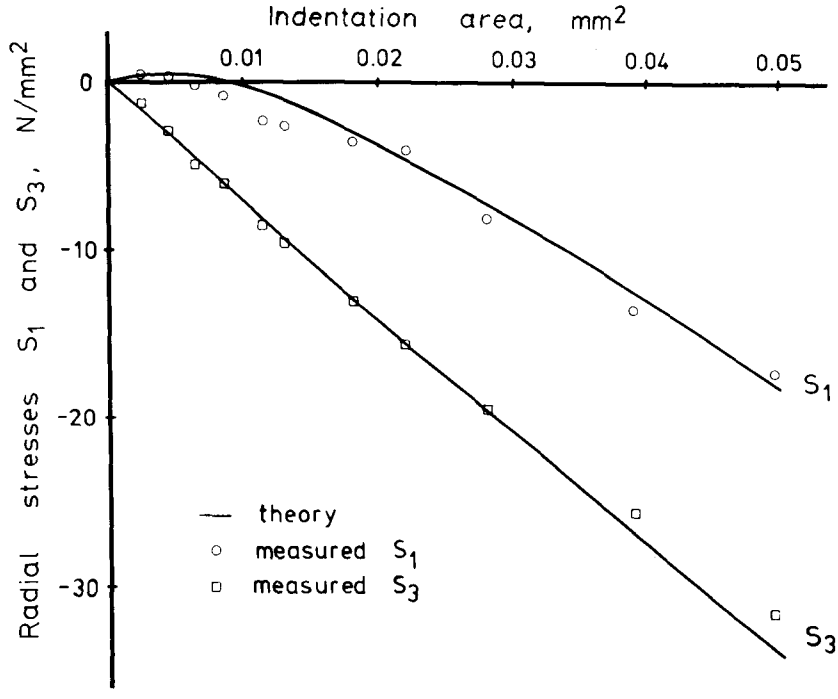

FIG. 7. Variation of stresses S_1 and S_3 with indentation area.

NATURAL FREQUENCIES

A 2-mm-thick disc was rolled using a 15 kN roller load at a mean roller path radius, $r_m = 170$ mm. Disc natural frequency measurements for the first five modes and also roller path indentation measurements were made after 1, 2, 4, . . . , 64 roller circuits. An HP 5423A Structural Dynamics Analyzer measured the natural frequencies of the disc when centrally clamped between 50-mm radius collars. Figure 8 shows the measured disc natural frequencies and the corresponding predicted values calculated using the stresses S_1 and S_3 from (13) and (14). These stresses were used as input data for a computer program (Schajer 1979) which estimates disc natural frequencies by the Rayleigh-Ritz method (Hildebrand 1965). The good agreement between the measured and predicted values in Fig. 8 demonstrates that both the roller-induced stresses and the resulting changes in disc frequencies have been realistically modelled.

There is some deviation of the zero and one nodal diameter mode frequencies for large indentation areas. This is caused by axi-symmetric buckling of the disc ("dishing") as a result of slightly unsymmetrical deformation in the roller path. Soedel (1973) showed that a change from a flat plate to a similar spherically curved shell, such as occurred here, causes an increase in natural frequency, particularly for the lowest frequency modes.

In industrial practice, circular saws are sometimes rolled close to their periphery so as to reduce sawblade tension. A large roller path radius $r_m = 170$ mm, $r_m/b = 0.85$, was especially chosen here so as to illustrate this "detensioning" phenom-

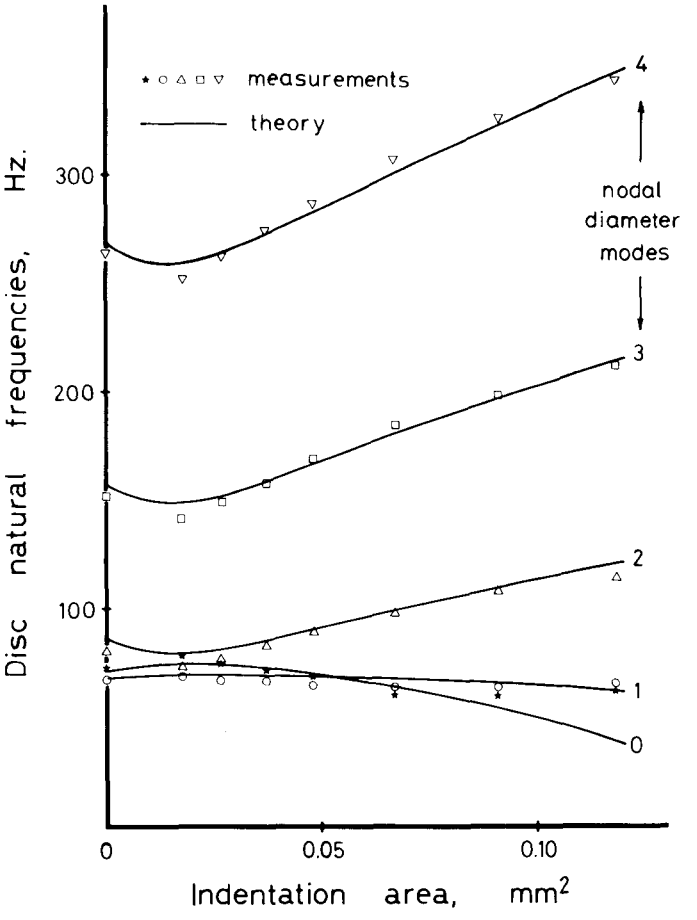

FIG. 8. Measured and calculated disc natural frequencies. Mean roller path radius, r_m = 170 mm.

enon. Under these conditions, the natural frequencies for modes $n \geq 2$ initially decrease, but subsequently increase after further rolling. This occurs because these vibration modes are mainly influenced by the circumferential membrane stresses. Initially, the very large circumferential compressive stress in the roller path, corresponding to the stress difference $S_3 - S_1$, (Eq. [4]), cause a decrease in the natural frequencies. Subsequently, the tensile circumferential stresses in region III, corresponding to the stress S_3 (Eq. [3]), grow sufficiently large to cause a net increase in the higher mode frequencies. For a smaller roller path radius, $r_m/b < 0.8$, the natural frequencies of modes $n \geq 2$ monotonically increase with increasing indentation. Region III is much larger than before and the effect of the tensile circumferential stresses within the region is always dominant.

The opposite behavior occurs for the $n = 0$ and $n = 1$ modes because they are mainly influenced by the radial membrane stresses. For a large roller path radius, region I and the associated stress S_1 are the dominant influences. Thus, the natural frequencies in these two modes initially increase and then decrease to reflect the shape of the S_1 curve in Fig. 7. For $r_m/b < 0.8$, region III and stress S_3 are

dominant. These natural frequencies then monotonically decrease to reflect the shape of the S_3 curve in Fig. 7.

The theoretical model developed in this study is successful in describing the changes in sawblade natural frequencies, even in the extreme case discussed here, because it accurately predicts the development of the tensioning stresses, notably the initially tensile stress S_1 and the difference between the stresses S_1 and S_3.

SAWBLADE STABILITY

As an example of the prediction of an optimal tensioning condition that maximizes sawblade stability, consider a circular sawblade with peripheral radius 200 mm, thickness 2.0 mm, clamping radius 50 mm and rotation speed Ω = 4,000 rpm. The rotation of this saw causes an apparent splitting of the blade natural frequencies relative to a ground-based observer, and critical speed instability occurs when the backward-travelling wave frequency, $\omega_n - n\Omega$, in any mode is equal or very close to zero (Mote and Nieh 1973). Figure 9(a) shows the backward-travelling wave frequencies of the sawblade when rolled at 50 mm radius, as a function of indentation area. These curves were calculated using the computer program SAWFQ2 (Schajer 1979) with the stresses from Eqs. (13) and (14). Thermal stresses also contribute to natural frequency changes, but for simplicity, these stresses are assumed zero here.

Marginally stable/unstable behavior is expected with the unstressed saw (zero indentation area), because the backward-travelling wave frequency for the 2 nodal diameter mode is almost zero. With very large indentations (indentation area > 0.14 mm^2), the 0 nodal diameter frequency is reduced to zero, and buckling ("dishing") of the sawblade occurs. An indentation area equal to 0.07 mm^2 can be identified as the optimal deformation at this roller path radius because it maximizes the lowest backward-travelling wave frequency. This criterion for the optimal induced stress condition was verified in production trials with circular saws, where sawblade natural frequencies were controlled by the deliberate induction of thermal membrane stresses, "thermal tensioning" (Mote et al. 1981).

Mean roller path radius is an additional variable that can be included in the rolling process optimization procedure. Figure 9 shows the sawblade natural frequency vs. indentation area curves for a range of roller path radii. Although the highest "optimal" frequencies are achieved by using a large roller path radius, it is probably not practical to roll a sawblade at a radius greater than about $r_m/b \approx 0.85$ because of the very large indentation areas which would then be required. The curves in Fig. 9 show that the potential increase in "optimal" frequency through the choice of roller path radius is not large. However, the curves also show that the indentation areas required to reach the optimal state for any given roller path radius varies over a wide range, and has a minimum at $r_m/b \simeq 0.5$. Similar observations have been reported by several investigators (Aoyama and Ohmori 1977; Kimura 1976; Kimura and Asano 1976; Pahlitzsch and Friebe 1974). However, this roller path radius is not "optimal" in the sense discussed here, because it is desired to optimize the effects of the roller-induced stresses, and not to minimize the sawblade deformation required to maximize the lowest backward-travelling wave frequency.

For $r_m/b = 0.85$, the "optimal" backward-travelling wave frequency is 34 Hz. To achieve a similar frequency with an untensioned saw, a plate thickness of

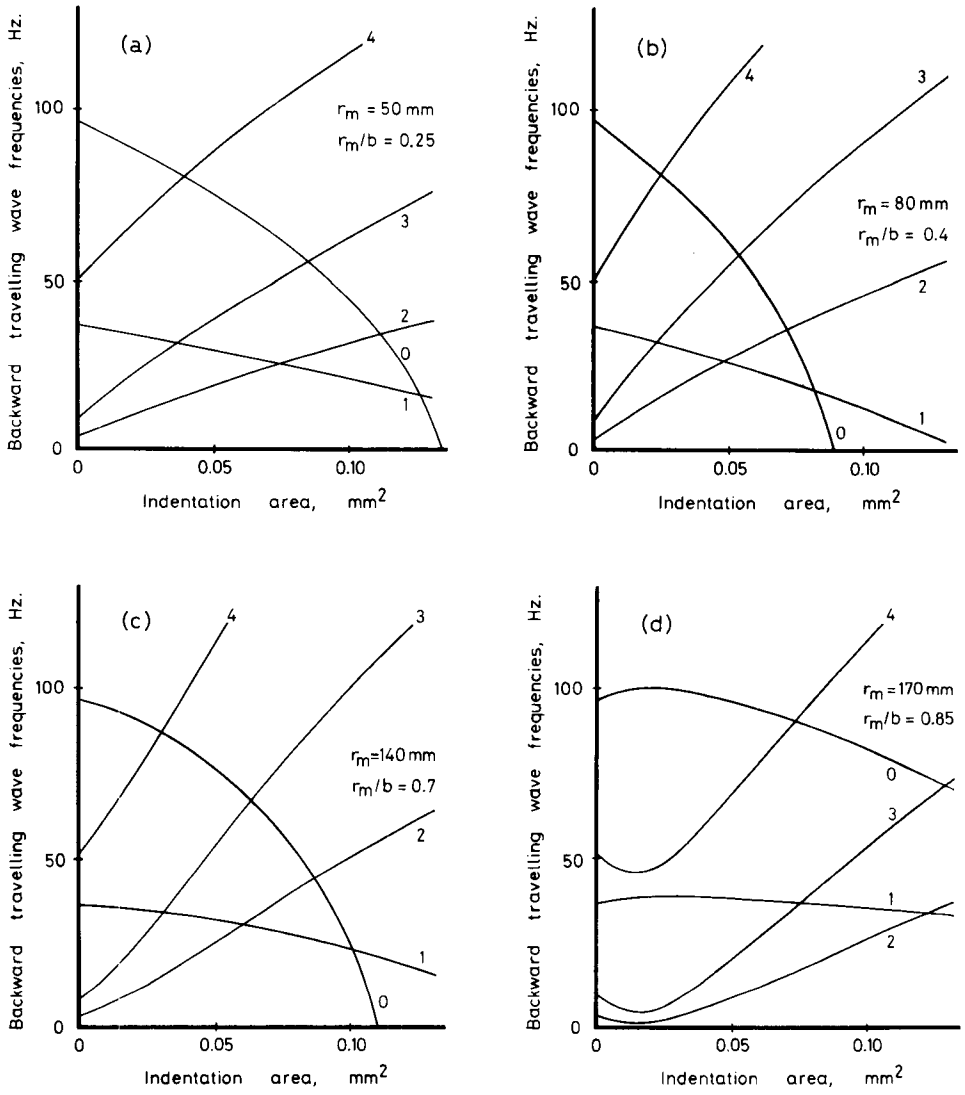

FIG. 9. Sawblade backward travelling wave frequencies vs. indentation area. Ω = 4,000 rpm. (a) r_m = 50 mm, r_m/b = 0.25; (b) r_m = 80 mm, r_m/b = 0.4; (c) r_m = 140 mm, r_m/b = 0.7; and (d) r_m = 170 mm, r_m/b = 0.85.

3.0 mm would be required instead of 2.0 mm. Thus, compared with an untensioned sawblade, a 33% thickness reduction can be achieved by proper tensioning.

CONCLUSIONS

The three-region model presented here accurately predicts the development of residual stresses in a roll-tensioned circular saw and the resulting changes in sawblade natural frequencies. This model is important for the reliable prediction of optimal rolling conditions and for the development of automated control of the tensioning process.

The cross-sectional area of the roller path indentation was used as a measure of the deformation that takes place during roll tensioning. Relationships between the indentation area and the tensioning stresses were derived and were verified by experimental stress measurements. Also, the predicted effects of these tensioning stresses on sawblade natural frequencies closely agreed with the experimental results.

Optimal tensioning conditions for a given saw operating environment are achieved when the lowest backward-travelling wave frequency is maximized. This frequency maximum can be closely approached by rolling the sawblade at any given roller path radius, providing that the roller path deformation is chosen appropriately. The model presented here shows how the roller path deformation can be chosen for any given roller path radius and saw operating environment, and how this deformation can be achieved in practice.

In an example case of an optimally tensioned circular sawblade, a 33% reduction in thickness was achieved compared with an untensioned circular sawblade with the same lowest backward-travelling wave frequency, and hence, the same dynamic stability.

REFERENCES

AOYAMA, T., AND Y. OHMORI. 1977. Tensioning of circular saw blade by stretcher. I. Effect of rolling position. (In Japanese) J. Jap. Wood Res. Soc. 23(6):280–285.

CLEPHANE, T. P., AND J. CARROLL. 1981. Timber: Even non-industry investors realize its value. For. Ind. 108(1):49–51.

DUGDALE, D. S. 1966. Theory of circular saw tensioning. J. Prod. Res. 4(3):237–248.

HARPOLE, G. B., E. WILLISTON, AND H. H. HALLOCK. 1979. Investment opportunity: The FPL EGAR lumber manufacturing system. Research Paper FPL 310. Forest Products Laboratory, Madison, WI.

HILDEBRAND, F. B. 1965. Methods of applied mathematics. Prentice-Hall, Englewood Cliffs, NJ. Chapter 2.

HILL, R. 1950. The mathematical theory of plasticity. Clarendon Press, Oxford. Chapter 2.

KIMURA, S. 1976. Studies on tensioning of circular saw by rolling pressure. 3. (In Japanese) J. Jap. Wood Res. Soc. 22(6):343–348.

———, AND M. ANDO. 1974. Studies on tensioning of circular saw by rolling pressure. 1. (In Japanese) J. Jap. Wood Res. Soc. 20(5):196–204.

———, AND I. ASANO. 1976. Studies on tensioning of circular saw by rolling pressure. 4. (In Japanese) J. Jap. Wood Res. Soc. 22(7):387–392.

MOTE, C. D., JR., AND L. T. NIEH. 1973. On the foundation of circular-saw stability theory. Wood Fiber 5(2):160–169.

———, G. S. SCHAJER, AND S. HOLØYEN. 1981. Circular saw vibration control by induction of thermal membrane stresses. J. Eng. Ind. 103(1):81–89.

PAHLITZSCH, G., AND E. FRIEBE. 1973. Über das Vorspannen von Kriessägeblattern. II. (On tensioning of circular sawblades. Part II) Holz Roh- Werkst. 31(12):457–463.

———, AND ———. 1974. Über das Vorspannen von Kriessägeblattern. III. (On the tensioning of circular sawblades. Part III) Holz Roh- Werkst. 32(1):5–12. Environment Canada Translation No. 844.

SCHAJER, G. S. 1979. Circular saw natural frequency program SAWFQ2. Technical Report 35.01.130, No. 13, University of California Forest Products Laboratory, Richmond, CA.

———. 1981. Analysis of roller-induced residual stresses in circular discs and their effect on disc vibration. Ph.D. dissertation, University of California, Berkeley, CA.

SOEDEL, W. 1973. A natural frequency analogy between spherically curved panels and flat plates. J. Sound Vibr. 29(4):457–461.

SZYMANI, R., AND C. D. MOTE, JR. 1979. Theoretical and experimental analysis of circular saw tensioning. Wood Sci. Technol. 13(3):211–237.

TAYLOR, G. I., AND H. QUINNEY. 1931. The plastic distortion of metals. Philosophical Transactions of the Royal Society, Series A. 230:323–362.